Study on the temporal coherence function of a femtosecond optical frequency comb

Dong Wei[*], Satoru Takahashi, Kiyoshi Takamasu, and Hirokazu Matsumoto
Department of Precision Engineering, University of Tokyo, Hongo 7-3-1,Bunkyo-ku, Tokyo
113-8656, Japan

ABSTRACT

The interference measurement using the femtosecond optical frequency comb (FOFC) is in progress at present. We analyzed the temporal coherence function (TCF) of an FOFC since which is the fundamental description of the interference phenomenon. As a result, it has been understood that the same high coherence peak exists during the time which is equal to the repetitions interval in the traveling direction of the FOFC. The theoretical derivation has been used to model the TCF of an FOFC and shows good agreement with experimental measurements which is taken with a combination of an ordinary Michelson interferometer and an unbalanced optical-path Michelson interferometer.

Keywords: Ultrafast phenomena, Mode-locked lasers, Coherence, Interferometry

1. INTRODUCTION

Femtosecond optical frequency comb (FOFC) based on a combination of mode-locked technique and stable frequency-control technique [1]. The increased frequency stability and the very broad frequency band of FOFC [2] has led to the application of this device in several precision metrology application areas such as precision optical frequency metrology, high-precision spectroscopy, and distance measurements. Minoshima and Matsumoto reported in 2000 that high temporal coherence between an adjacent pair of pulse trains from an FOFC for length measurement [3]. Following that pioneering work, various experiments were proposed using high temporal coherence between a pair of pulse trains for measurement of the group refractive index of air [4, 5], absolute measurement of long distance [6-8], and precision surface-profile metrology [9, 10].

Interferometric measurements using FOFC are in progress at present, all of which put stringent demands on the high temporal coherence of the FOFC source. To the best of our knowledge, few studies have been carried out regarding the temporal coherence function (TCF) of a pulse train from an FOFC, though such an FOFC is likely to be useful for metrology applications.. And we notice that the usage of high temporal coherence in these experiments is restricted to a pair of pulse trains. An earlier study [11] considered the temporal coherence function of an FOFC

In the present study, we make an attempt to demonstrate a modified Michelson interferometer to observe same high temporal coherence peaks between different paris of pulse trains from an FOFC. As be shown below, this technique maintains the simplicity of the equipments. For simplicity of explanation, we have neglected the dispersion and absorption of the optical elements over the FOFC's illumination bandwidth.

2. PRINCIPLES

2.1 TCF of FOFC

Note that the TCF of an FOFC is essential for the experiments mentioned above. In what follows, for convenience of explanation, let us first consider the TCF of an FOFC.

---

[*] weidong@nanolab.t.u-tokyo.ac.jp; phone +81 3-5841-6472; fax +81 3-5841-6472; http://www.nanolab.t.u-tokyo.ac.jp/xindex.html
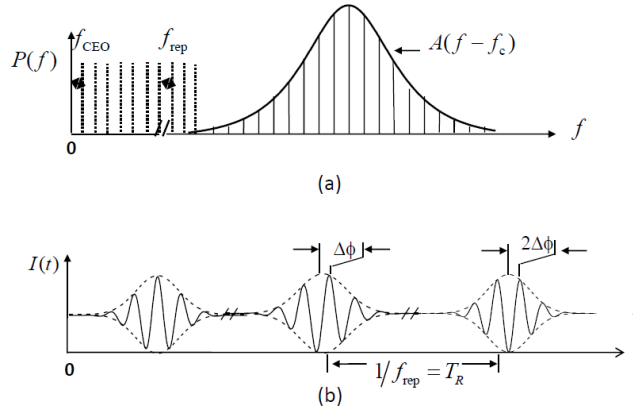
Fig. 1. Fourier-transform relationship between the power spectrum and the interference fringes. (a) Power spectrum of the FOFC. (b) Interference fringes; dotted line: the temporal coherence function of the FOFC; solid line: interference fringes.

The power spectrum of an FOFC light source can be expressed as [11]

$$P(f) \propto A(f - f_c) \times \sum_{m=-\infty}^{+\infty} \delta(f - mf_{rep} - f_{CEO}),$$ (1)

where $A(f - f_c)$ is the envelope function of the FOFC power spectrum, f_c is the center carrier frequency of the FOFC. When the electric field packet repeats at the pulse repetition period T_R, the "carrier" phase slips by $\Delta\varphi_{ce}$ to the carrier-envelope phase because of the difference between the group and phase velocities. In the frequency domain, a mode-locked FOFC generates equidistant frequency comb lines with the pulse repetition frequency $f_{rep} \propto 1/T_R$, and due to phase slip $\Delta\varphi_{ce}$, the whole equidistant-frequency comb is shifted by f_{CEO}.

Based on the Wiener–Khintchine theorem, the interferometric signal of the autocorrelation function is given by the inverse Fourier transform of the spectrum of the source, and we have

$$\gamma(\tau) \propto F^{-1}\left[A(f - f_c)\right] \otimes \sum_{m=-\infty}^{+\infty} \delta(\tau - mT_R).$$ (2)

From Eq. (2), the TCF periodically displays a same high temporal coherence peak where the pulse trains signal of the FOFC displays a high-intensity peak with the pulse repetition period T_R

2.2 Interference fringes' formation
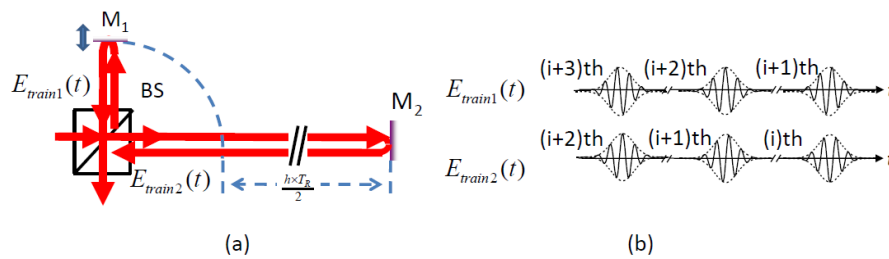
Fig. 2. Relative delay between pulse trains formed by an unbalanced optical-path Michelson interferometer (a) Simplified optical layout for interferometry. (b) Relative positions between two pulse trains (integer h=1).

Let us consider the interference fringes formed by an unbalanced optical-path Michelson interferometer, as shown in Fig. 2(a). First, the incoming pulse trains is split into two identical parts, $E_{\text{train}1}(t)$ and $E_{\text{train}2}(t)$ at the beam splitter BS, relatively $E_{\text{train}2}(t)$ delays to $E_{\text{train}1}(t)$ and they finally are recombined at the BS (see Fig. 2(b)).

The intensity due to the linear superposition of N pulse pairs from $E_{train1}(t)$ and $E_{train2}(t)$ with parallel polarization is just

$$I(t) \propto \sum_{i=1}^{N} \left\langle \left| E(t) \right|^2 \right\rangle \tag{3}$$

$$
\begin{aligned}
\left| E(t) \right|^2 &= \left| \frac{1}{2} E_{train1}(t) + \frac{1}{2} E_{train2}(t+\tau) \right|^2 \\
&= \left| \frac{1}{2} E_{train1}(t) \right|^2 + \left| \frac{1}{2} E_{train2}(t+\tau) \right|^2 + \frac{1}{4} E^{*}{}_{train1}(t) E_{train2}(t+\tau) + \frac{1}{4} E_{train1}(t) E^{*}{}_{train2}(t+\tau) \quad (4) \\
&\propto \left| \gamma(\tau) \right| \cos(\text{mod}(h \times \Delta\varphi_{ce}, 2\pi))
\end{aligned}
$$

where $\text{mod}(h \times \Delta\varphi_{ce}, 2\pi)$ returns $h \times \Delta\varphi_{ce} - n \times 2\pi$ and $n = \text{floor}(h \times \Delta\varphi_{ce}/2\pi)$ ($\text{floor}(h \times \Delta\varphi_{ce}/2\pi)$ rounds the elements of $h \times \Delta\varphi_{ce}/2\pi$ to the nearest integers less than or equal to $h \times \Delta\varphi_{ce}/2\pi$), hT_R is the relative delay between $E_{train1}(t)$ and $E_{train2}(t)$, $\Delta\varphi_{ce}$ is the "carrier" phase slip as shown in Fig. 1(a). After performing the time integration we obtain

$$I(t) \propto \left| \gamma(\tau) \right| \sum_{i=1}^{N} \left\langle \cos(\text{mod}(h \times \Delta\varphi_{ce}, 2\pi)) \right\rangle. \tag{5}$$

A question is whether one can obtain the interference fringes, since measurement time is a little long and average of the pulse trains is typically a large number. In the case of a pulse trains from an FOFC, the mode-lock technique results in interference fringes reappearing at delays equal to hT_R an integer h multiple of the pulse repetition period T_R. And the information about the time-averaged value first provides $\left\langle \cos\left[\text{mod}(h \times \Delta\varphi_{ce}, 2\pi) \right] \right\rangle = \cos\left[\text{mod}(h \times \Delta\varphi_{ce}, 2\pi) \right]$ ($\langle \ \rangle$ denotes time integration over the pulse envelope and carrier period) by Xu et al [12]. When the pulse trains $E_{\text{train}1}(t)$ and the relatively delayed pulse trains $E_{\text{train}2}(t)$ overlap in space, one would expect that interference fringes can be observed, as shown in Fig. 1(b). After performing the time integration we obtain

$$I(t) \propto \left| \gamma(\tau) \right| \cos[\text{mod}(h \times \Delta\varphi_{ce}, 2\pi)]. \tag{6}$$

3. COMPUTER EXPERIMENT

To confirm the principle described above, the computation simulations is carried out with an FOFC with the pulse duration of 180 femtoseconds. The repetition rate of the FOFC source is 100MHz. The output wavelength of the pulse is centered at 1550 nm with a bandwidth of 20 nm. For simplicity of explanation, we assume the power spectrum distribution is a Gauss function.
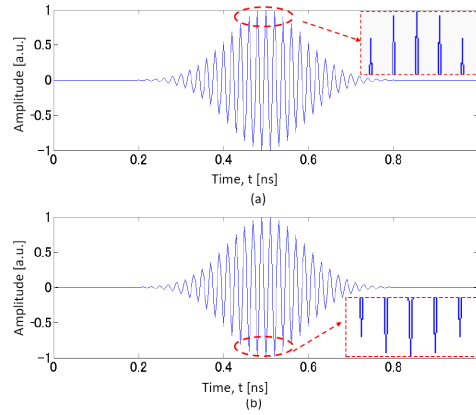
Fig. 3. Calculated optical pulses carried out with an FOFC. (a) $\Delta\phi = 0\,[rad]$.(b) $\Delta\phi = \pi\,[rad]$.

Figure 3 illustrates the calculated optical pulses with different carrier phase slip.
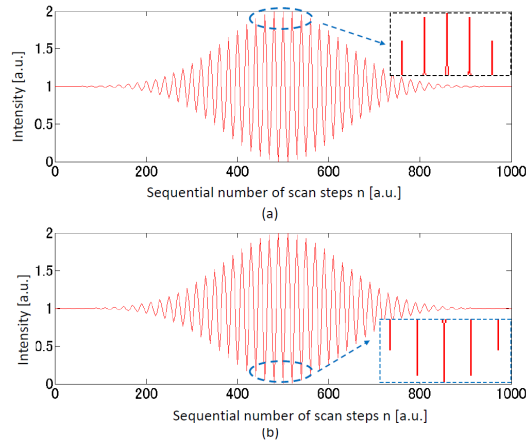
Fig. 4. Interference fringes. (a) $\Delta\phi = 0\,[rad]$.(b) $\Delta\phi = \pi\,[rad]$ ..

In Fig. 4 we show acquire Interference fringes between the different pairs of pulses according to Eq. (6). The conventional white-light interferometry introduced Interference fringes are shown in Fig. 5(a). And the unbalanced optical-path Michelson interferometer (between different pulses with a carrier phase slip π) introduced Interference fringes are shown in Fig.5 (b). We can confirm the carrier phase slip π between Interference fringes as shown in Fig. 6.

From the above computation simulation, the TCF of an FOFC and interference fringes formation between pulses with different carrier phase slip, as described in principle, are confirmed.

4. EXPERIMENT

The experimental setup is simple, and its optical schematic is illustrated in Fig. 5. The experiment is carried out with a system consisting of a polarization-mode-locked femtosecond fiber laser (FC1500, MenloSystems), a modified Michelson interferometer, and system control. The pulse duration, repetition rate, and total output power of the fiber

laser are 180 femtosecond, 100 MHz, and 20 mW, respectively. The output wavelength of the pulse is centered at 1550 nm with a bandwidth of 20 nm.

The pulse train from the FOFC is expanded and collimated by a collimator C and introduced into a modified Michelson interferometer. The modified Michelson interferometer is a combination of an ordinary Michelson interferometer and two unbalanced optical-path Michelson interferometers as introduced in the principles. The ordinary Michelson interferometer is composed of a beam splitter BS, a reference mirror M_1, and an object mirror (half-reflection mirror) HM_1. One unbalanced optical-path Michelson interferometer is composed of the common BS and M_1, and a different object mirror (half-reflection mirror) HM_2. The other unbalanced optical-path Michelson interferometer is composed of the common BS and M1, and a different object mirror M_2. The mirrors HM_2 and M_2 are arranged at space position far away from HM_1 about 1.5 m and 3 m in space, respectively.
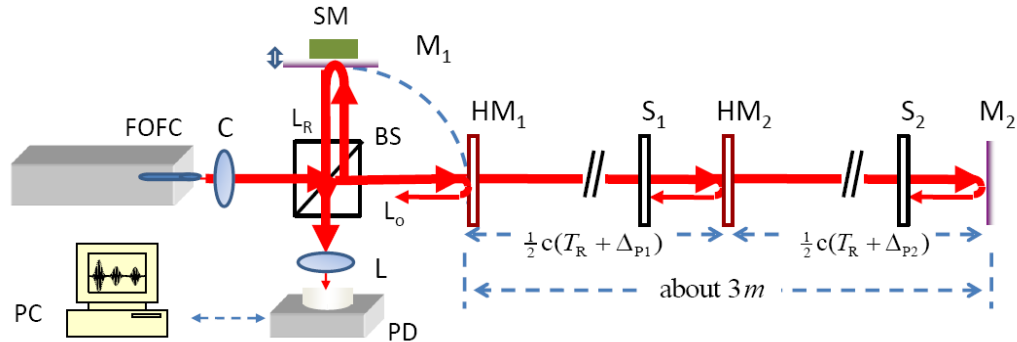
Fig. 5. Optical schematic. FOFC: femtosecond optical frequency comb, C: collimator, L: Lens, BS: beam splitter, PD: photo detector, SM: ultrasonic stepping motor, HM_{1-2}: half mirror, S_{1-2}: shutter, M_{1-2}: mirror, PC: computer.
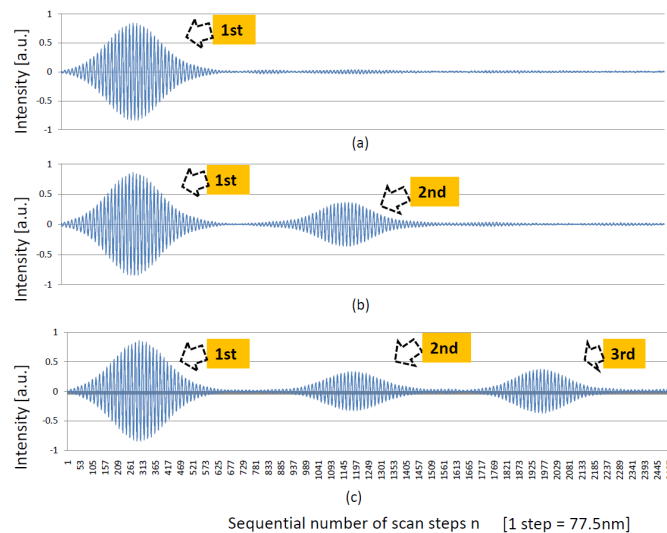
Fig. 6. Interference fringes at three different situations. (a) Shutter S_1 is closed. (b) Shutter S_1 is opened and S_2 is closed. (c) Shutter S_1 and S_2 are opened.

The pulse train is split into two identical parts at the beam splitter BS. One part of the pulse train goes into the common reference arm of the three interferometers with length L_R and is reflected by mirror M_1. The other part of the pulse train goes into the other arm with lengths Lo, $Lo+cT_R+c\Delta_{P1}$, and $Lo+2cT_R+c\Delta_{P1}+c\Delta_{P2}$ (c is the light velocity in air.) and are sequentially reflected by mirrors HM_1, HM_2, and M_2, respectively. The displacement $c\Delta_{P1}$ and $c\Delta_{P2}$ are

introduced to avoid overlap with each other between interference fringes in space. During the measurement, by moving the common reference arm of the interferometers by means of a computer-controlled and calibrated ultrasonic stepping motor (TULA-OP-03, Technohands, Inc), we could vary the relative delay between the two output pulse trains of the three pairs.

After traveling different path lengths, these three pairs of pulse trains sequentially overlap at the beam splitter. Lens L images the interference fringes onto a photo detector PD (Front-end optical receivers Model 2011, New Focus, Inc.). The intensity of the interference fringes signal through PD is measured with a digital oscilloscope (TDS1000B, Tektronix, Inc.) and is sent to a computer PC.

In Fig. 6 we show the acquired interference fringes recorded in three different situations. The 2nd and 3rd interference fringe peaks appear when the shutters S_1 and S_2, respectively, are opened. As predicted, the interference fringe signals exhibit a high contrast between the two pairs of pulse trains by the relative displacements $cT_R+c\Delta_{P1}$ (about 1.5 m) and $2cT_R+c\Delta_{P1}+c\Delta_{P2}$ (about 3 m).

Theoretically, including the calculation of the intensity change with the half mirror, the three peaks should have the same height value according to Eq. (6). The experimental measurements are achieved by displaying three interference fringe signals to one screen of a oscilloscope in order to shorten the measurement time and suppress the influence due to air turbulence and mechanical vibration. The measurement results primarily suffer from the error arising from peak overlap caused by side lope noise on interference fringes due to the restricted resolution of the oscilloscope. The performance can be improved by removing the shutters S_1 and the mirror HM_2.
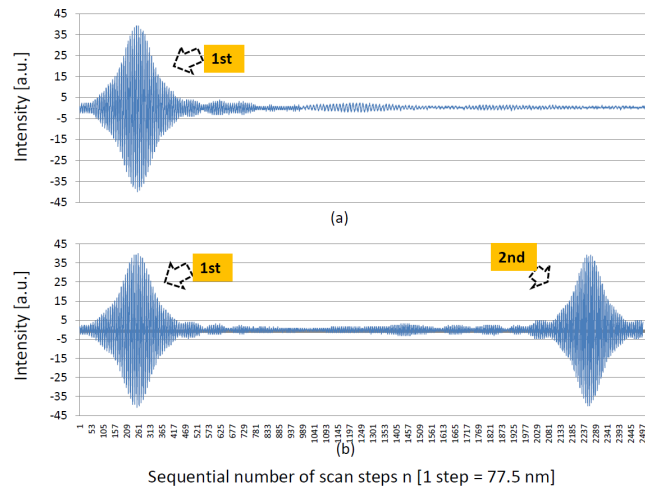
Fig.7. Interference fringes with different relative delays between two pulse trains. (a) Shutter S_2 is cloesd. (b) Shutter S_2 is opened.

Figure 7 illustrates the acquire interference fringes recorded in two different situations after removing the shutters S_1 and the mirror HM_2. The 2nd interference fringes peak appears, when the shutter S_2 is opened. As predicted, because two interference fringe signals are sufficiently separated, figure 7 shows that the two peaks have the same height value.

To obtain the peak value of the two peaks we analyzed the fringes pattern in Fig. 7 by the Fourier transform technique [11]. And an approximate envelope curve was fitted to the obtained the TCF in order to obtain accurate peak values. Figure 8 demonstrates that obtained time average information of peak values between two peaks. There is a good agreement between the experimental data and the theory. The difference of the peak value between two peaks is equal to the resolution of the used digital oscilloscope.
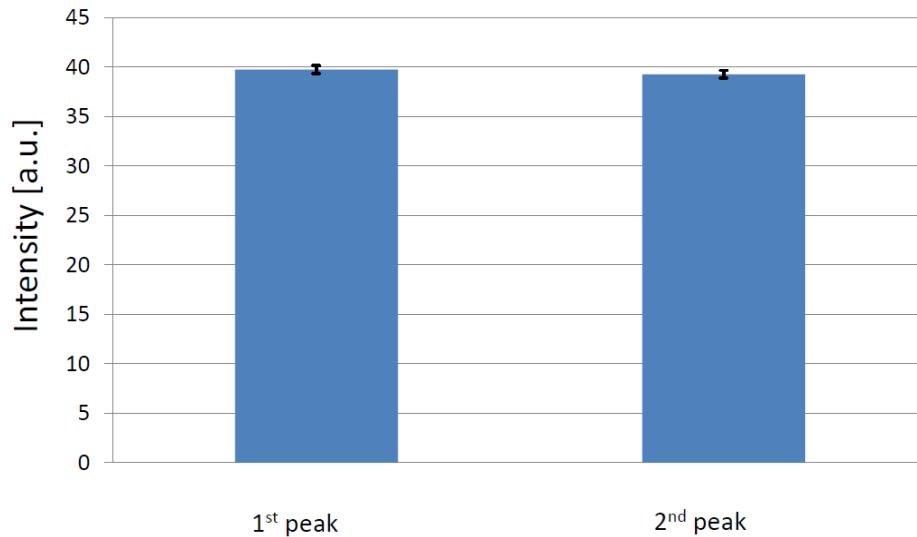
Fig.8 Time average of peak values

5. SUMMARY AND FUTURE WORK

5.1 Summary

In closing, we have studied the TCF of FOFC. The results show that same high temporal coherence peaks exist during the period equal to the repetitions interval in the traveling direction of the used FOFC. The theoretical derivation of the expected temporal coherence function and the interference fringes agrees with the results of a simple proof-of-the-principle experiment using a modified Michelson interferometer with optical path differences up to 6m. And there is a good agreement between the experimental data and the theory. Based on this new understanding of the TCF of FOFC, new applications can be proposed fairly readily.

5.2 Future work

As is known well, the amount of the change of the refractive index of air is about 0.9 ppm when the temperature of the surrounding air changes by 1 degree. Because of sensitivity to variations in temperature, when the temperature of the air changes, the refractive index of air changes, and consequentially the relative optical path difference between mirrors changes. In future work, by making the best use of the unique temporal coherence characteristic of FOFC, we plan to propose a brand-new interferometer that can considerably measure the average temperature change over lager distance between mirrors [13].

ACKNOWLEDGMENTS

REFERENCES

[1] T. Udem, R. Holzwarth, and T. W. Hansch, "Optical frequency metrology," Nature **416**, 233-237 (2002).
[2] J. Ye, and S. T. Cundiff, Femtosecond optical frequency comb : principle, operation, and applications (Springer, New York, NY, 2005).
[3] K. Minoshima, and H. Matsumoto, "High-Accuracy Measurement of 240-m Distance in an Optical Tunnel by Use of a Compact Femtosecond Laser," Appl. Opt. **39**, 5512-5517 (2000).
[4] Y. Yamaoka, K. Minoshima, and H. Matsumoto, "Direct Measurement of the Group Refractive Index of Air with Interferometry between Adjacent Femtosecond Pulses," Appl. Opt. **41**, 4318-4324 (2002).
[5] J. Zhang, Z. H. Lu, and L. J. Wang, "Precision refractive index measurements of air, N-2, O-2, Ar, and CO2 with a frequency comb," Applied Optics **47**, 3143-3151 (2008).
[6] T. Yasui, K. Minoshima, and H. Matsumoto, "Stabilization of femtosecond mode-locked Ti:sapphire laser for high-accuracy pulse interferometry," IEEE Journal of Quantum Electronics **37**, 12-19 (2001).
[7] J. Ye, "Absolute measurement of a long, arbitrary distance to less than an optical fringe," Opt. Lett. **29**, 1153-1155 (2004).
[8] M. Cui, R. N. Schouten, N. Bhattacharya, and S. A. Berg, "Experimental demonstration of distance measurement with a femtosecond frequency comb laser," Journal of the European Optical Society - Rapid publications **3**, 08003 (2008).
[9] J. S. Oh, and S. W. Kim, "Femtosecond laser pulses for surface-profile metrology," Opt. Lett. **30**, 2650-2652 (2005).
[10] S. Kray, F. Spöler, M. Först, and H. Kurz, "Dual femtosecond laser multiheterodyne optical coherence tomography," Opt. Lett. **33**, 2092-2094 (2008).
[11] Dong Wei, Satoru Takahashi, Kiyoshi Takamasu, and Hirokazu Matsumoto, "Analysis of the temporal coherence function of a femtosecond optical frequency comb," Opt. Express 17, 7011-7018 (2009)
[12] L. Xu, C. Spielmann, A. Poppe, T. Brabec, F. Krausz, and T. W. Hansch, "Route to phase control of ultrashort light pulses," Opt. Lett. **21**, 2008-2010 (1996).
[13] D. Wei, S. Takahashi, K. Takamasu, and H. Matsumoto, to be published in Jpn. J. Appl. Phys.